University of Wollongong

Research Online

Faculty of Engineering - Papers (Archive)

Faculty of Engineering and Information Sciences

2012

Monte Carlo study of the potential reduction in out-of-field dose using a patient-specific aperture in pencil beam scanning proton therapy

Stephen J. Dowdell
University of Wollongong, sjd431@uow.edu.au

Benjamin Clasie
Massachusetts General Hospital and Harvard Medical School

Nicolas Depauw
University of Wollongong, nd999@uowmail.edu.au

Peter E. Metcalfe
University of Wollongong, metcalfe@uow.edu.au

Anatoly B. Rosenfeld
University of Wollongong, anatoly@uow.edu.au

See next page for additional authors

Follow this and additional works at: https://ro.uow.edu.au/engpapers

Part of the Engineering Commons

https://ro.uow.edu.au/engpapers/4602

Recommended Citation

Authors

Stephen J. Dowdell, Benjamin Clasie, Nicolas Depauw, Peter E. Metcalfe, Anatoly B. Rosenfeld, Hanne M. Kooy, Jacob B. Flanz, and Harald Paganetti

Monte Carlo study of the potential benefit of using a patient-specific aperture in pencil beam scanning proton therapy

S J Dowdell[1,2], B Clasie[2], N Depauw[1,2], P Metcalfe[1], A B Rosenfeld[1], H M Kooy[2], J Flanz[2] and H Paganetti[2]

[1] Centre for Medical Radiation Physics, University of Wollongong, Wollongong, NSW 2522 Australia

[2] Department of Radiation Oncology, Massachusetts General Hospital & Harvard Medical School, Boston MA 02114

Abstract

This study aimed at identifying the potential benefits of using a patient specific aperture in proton beam scanning. For this purpose an accurate Monte Carlo model of the pencil beam scanning (PBS) proton therapy (PT) treatment head at Massachusetts General Hospital (MGH) was developed based on an existing model of the passive double-scattering (DS) system. The Monte Carlo code specifies the treatment head at MGH with sub-millimeter accuracy. The code was configured based on the results of experimental measurements performed at MGH. This model was then used to compare out-of-field doses in simulated double-scattering (DS) treatments and PBS treatments

For the conditions explored, the penumbra in PBS is wider than in DS, leading to higher absorbed doses and equivalent doses adjacent to the primary field edge. For lateral distances greater than 10cm from the field edge, the doses in PBS appear to be lower than those observed for DS.

23 We found that placing a patient-specific aperture at nozzle exit during PBS treatments can potentially

24 reduce doses lateral to the primary radiation field by over an order of magnitude. In conclusion, using

25 a patient-specific aperture has the potential to further improve the normal tissue sparing capabilities of

26 PBS.

27

28 Keywords: proton therapy, pencil beam scanning, Monte Carlo simulation, patient-specific aperture

29

30 **1. Introduction**

31 Pencil beam scanning (PBS) proton therapy (PT) has the potential to deliver highly conformal fields

32 with reduced dose external to the primary field compared to double scattering (DS) PT. In PBS,

33 magnets are used to scan the proton beam laterally and the energy of the proton beam is typically

34 altered without beam modifying devices to achieve conformality in three dimensions. In contrast to

35 DS, PBS has the ability to conform the dose to both the proximal and distal edges of the target

36 (Lomax *et al.*, 2004). PBS treatments can also be delivered without patient-specific hardware, which

37 is required to achieve conformality to the lateral and distal edges of the target in DS (Kooy *et al.*,

38 2010). Not using patient-specific hardware reduces the amount of material in the path of the beam,

39 which decreases the total number of proton interactions occurring in the treatment nozzle, leading to a

40 lower neutron dose from PBS (Schneider *et al.*, 2002). The definition of in-field used in this work is

41 the region traversed by primary protons (including penumbra), while out-of-field is defined as the

42 dose delivered by secondary particles in the region not traversed by primary particles.

43 There are two principle methods of beam scanning used in PT, which we define as spot scanning and

44 continuous scanning. Spot scanning involves delivering dose in a series of finite steps. After the

45 delivery of each spot, the beam is turned off while the elements which steer the beam are reconfigured

46 to deliver the next spot. This reconfiguration may require a change in the beam position, energy or

47 both depending on the individual facility and the chosen scanning methodology. The primary

48   difference between continuous scanning and spot scanning is that during continuous scanning, the

49   beam remains on while the position is altered. Scanning fields at MGH are delivered via a series of

50   two-dimensional layers of constant proton energy (and hence range). The distal layer is irradiated

51   first, then the energy is reduced and the subsequent layer irradiated. This process continues until the

52   entire field has been delivered. Other PT centers may use a different scanning method, depending on

53   the hardware properties of the given facility.

54   Previous work by Paganetti *et al* (2004) has demonstrated the ability to accurately simulate DS proton

55   therapy treatments using the Geant4 Monte Carlo toolkit (Agostinelli *et al.*, 2003). Modeling the DS

56   treatment nozzle with sub-millimeter accuracy allowed the simulation of dose distributions from

57   spread out Bragg peak (SOBP) fields with accuracy, in terms of range and modulation, on the order of

58   a millimeter. Previous studies have also employed Monte Carlo for examination of the dose delivered

59   by primary and secondary particles (Paganetti, 2002, Dowdell *et al.*, 2009, Perez-Andujar *et al.*, 2009,

60   Zacharatou Jarlskog *et al.*, 2008, Zacharatou Jarlskog and Paganetti, 2008b). There is also potential in

61   the use of Monte Carlo simulations for patient specific dose calculation (Paganetti *et al.*, 2008).

62   The aim of this work was to study the feasibility and potential benefit of incorporating a patient-

63   specific aperture at nozzle exit during delivery of PBS fields. To achieve this we have implemented a

64   model of the PBS treatment head at the Francis H Burr Proton Therapy Center, Massachusetts

65   General Hospital (MGH) using the Geant4 Monte Carlo toolkit. The model was used to simulate the

66   doses in PBS PT. The results of these simulations were compared to simulations of the DS treatment

67   head at MGH.

68

69   **2. Method**

70   *2.1. Monte Carlo modeling of a PBS nozzle*

71 *2.1.1. Nozzle Geometry.* The components of the PBS nozzle jointly developed by MGH and IBA (Ion

72 Beam Applications, Louvain La Neuve, Belgium) were modeled in the Geant4 code (version

73 4.9.0.p01)). The geometry as implemented in the Monte Carlo code is shown in figure 1.
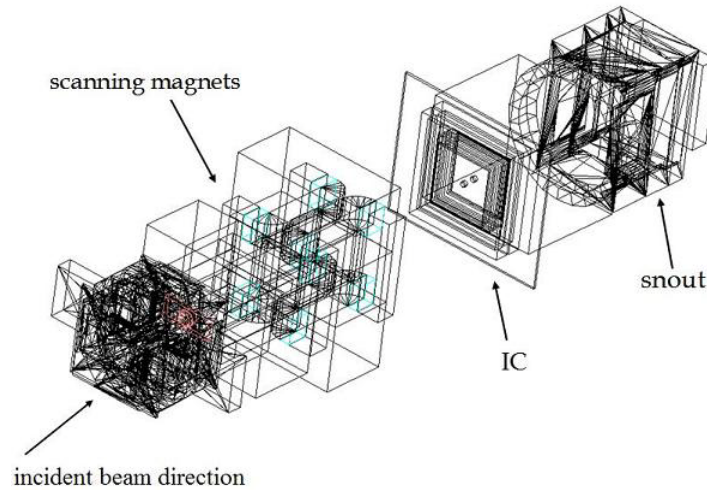
74

75 **Figure 1: The pencil beam scanning treatment head implemented in the Monte Carlo code,**

76 **showing the incident beam direction, scanning magnets, ionization chambers (IC) and the snout.**

77 Protons are generated in the simulations at the entrance of the treatment head. Upon entering the

78 treatment head, the beam passes through the first and second scanning magnets, which are used to

79 scan the proton pencil beam horizontally and vertically respectively. The Monte Carlo code reads in

80 the prescribed lateral spot positions and proton energy at the treatment head exit via an input file

81 which is directly generated by the treatment planning system (TPS). These parameters are translated

82 into magnetic field settings using an automated script which converts the prescribed lateral position to

83 the required field strength in both scanning magnets based on the proton mass, the proton energy of

84 the current layer and the required deviation from the central axis. Using the file generated by the TPS

85 ensures that the beam moves throughout a single two-dimensional layer with the same scanning

86 pattern in the simulation and the clinical delivery. The three-dimensional dose distribution is delivered

87 in a series of two-dimensional layers of constant energy (and hence range). The layers are delivered

88 sequentially, commencing with the distal layer (highest proton energy) and concluding with the most

89 proximal (lowest proton energy) layer. The specification of the spot positions and the beam current

90 delivered in the input file also determines whether spot scanning or continuous scanning is delivered.

91 The magnetic fields generated by the scanning magnets are modeled as uniform fields inside the

92 magnet volume and the magnetic field strength set to zero external to the magnet volume. The field

93 centers are defined based on drawings provided by the manufacturer (Ion Beam Applications) and the

94 field lengths are defined by the effective lengths of the two scanning magnets. This same

95 methodology was also used for the specification of the magnetic fields in the study of Peterson *et al*

96 (2009).

97 As protons, or secondary particles, traverse the magnetic fields, their maximum step size in the Monte

98 Carlo was restricted to 2mm. Monte Carlo simulations typically model particle trajectories as a series

99 of straight lines and restricting the maximum step ensures more accurate modeling of the curved

100 trajectory of charged particles through the magnetic fields. Elsewhere in the treatment head, the

101 maximum step size was set to 100mm as high accuracy modeling of the trajectories was not important

102 in these areas of the treatment head and reducing the maximum step size would increase simulation

103 time. All particle interactions with different elements of the treatment head were still modeled, as the

104 particles trajectory and information (energy, momentum etc) are recalculated by default in Geant4

105 when crossing volume boundaries. It is thus unlikely that a particle travels up to the maximum step

106 size without changing its direction or energy.

107 After passing through the scanning magnets, the beam then passes through the ionization chambers,

108 which are used to monitor spot position and particle fluence. It is imperative to include the ionization

109 chambers in the model of a PBS nozzle as proton interactions with the chambers can result in wide-

110 angle scatter.

111 Finally, the beam passes through the snout, which can be used to hold a patient-specific aperture.

112 Each of the different snout sizes available in the clinic which were previously modeled in the Monte

113 Carlo for the DS system (Paganetti *et al.*, 2004) can also be included in the PBS simulation code. In

114   the design of the treatment head it was suspected that there may be clinical PBS cases in which

115   patient-specific apertures or compensators are required (Kooy *et al.*, 2010). Examples of such cases

116   would include treatments of tumors located in close proximity to critical structures (e.g. spinal

117   column) where an aperture or range compensator could be used to sharpen the lateral or distal

118   penumbrae respectively. The Monte Carlo code also has the capability of including these patient-

119   specific devices.

120   *2.1.2. Definition of the proton phase space at treatment head entrance.* It has been shown previously

121   that the phase space at nozzle entrance can be modeled using four parameters (energy, energy spread,

122   geometrical sigma, and angular spread) and that these parameters can be treated independently for DS

123   delivery simulations (Paganetti *et al.*, 2004). It was also shown that the beam delivery was insensitive

124   to small variations in these parameters. However, PBS delivery can be expected to be more sensitive

125   due to the lack of a scattering system. In this work, Twiss parameters are used in the Monte Carlo to

126   govern the emission of protons at nozzle entrance. The Twiss parameters (α, β, γ) are calculated from

127   a solution to the first order equation of motion. For an equation of the form

128
$$\frac{d^2 x}{ds^2} + k_x(s) = 0 \tag{1}$$

129   there exists a general solution of the form

130
$$x(s) = \sqrt{\varepsilon \beta(s)} \cos(\psi(s) + \phi) \tag{2}$$

131   where ε and ϕ are arbitrary constants. Taking the derivative of equation 2 with respect to *s* yields

132
$$\begin{aligned} x'(s) &= \sqrt{\frac{\varepsilon}{\beta(s)}} \frac{\beta'(s)}{2} \cos(\psi(s) + \phi) - \sqrt{\varepsilon \beta(s)} \left(\sin(\psi(s) + \phi) \frac{1}{\beta(s)} \right) \\ &= -\sqrt{\frac{\varepsilon}{\beta(s)}} (\alpha(s) \cos(\psi(s) + \phi) + \sin(\psi(s) + \phi)) \end{aligned} \tag{3}$$

133   where

134
$$\psi(s)=\int_0^s \frac{d\tau}{\beta(\tau)}, \quad \alpha(s)\equiv -\frac{\beta'(s)}{2} \qquad \text{and } \gamma(s)\equiv \frac{1+\alpha(s)^2}{\beta(s)} \qquad (4)$$

135 The Twiss parameters govern the position and angular deviation of the protons generated in the Monte

136 Carlo simulations. The emittance is given by

137
$$\varepsilon = \gamma(s)^2 + 2\alpha(s)xx' + \beta(s)x'^2 \qquad (5)$$

138 and thus it is related to the area covered by the x, x' phase space ellipse shown in figure 2. Gaussssian

139 distributions ($\sigma = \sqrt{\varepsilon\beta}$) are assumed for the position and angular deviation.

140
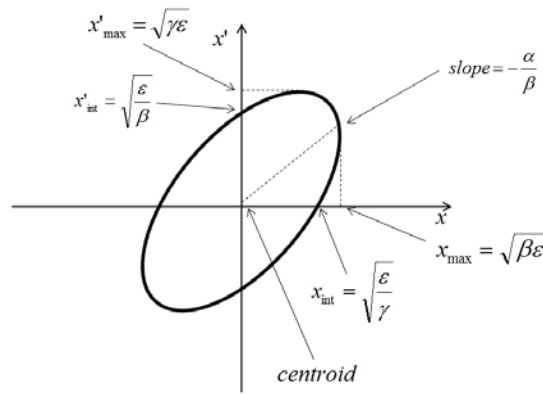
141

142 **Figure 2: A two-dimensional ellipse of area $\pi\varepsilon$ based on the Twiss parameters α, β and γ.**

143 The Twiss parameters incorporated into the Monte Carlo code are functions of range, R (g/cm^2), and

144 vary quadratically in a drift space. The variation in range arises from the increased lateral scattering

145 as the proton energy (and momentum) is decreased. Additionally, lower energy beams have a wider

146 momentum distribution, due to increased range straggling.

147 Initial values of the Twiss parameters were obtained from a transport calculation on the clinical

148 beamline (Rohrer, 2007, Brown *et al.*, 1980). Manual optimization of width of the Gausssian

149 distributions of position and angular distribution was performed such that the spot size obtained at

150 isocenter in air in simulations of different proton beam energies matched the results obtained from

151   measurements at the clinical PBS system at MGH using a Wellhofer MatriXX detector (IBA

152   Dosimetry).

153   The Twiss parameters (α,β,γ) together with the emittance (ε) describe the beam trajectory at the

154   nozzle entrance. The initial energy of the proton is defined by the range required (specified in input

155   file from TPS) and the calculated initial energy spread distribution at nozzle entrance.

156   *2.1.3. Geant4 physics models.* The different physics models available in the Geant4 toolkit were

157   compared in a previous study by Zacharatou Jarlskog and Paganetti (Zacharatou Jarlskog and

158   Paganetti, 2008a) with the aim of finding the best models for use in Monte Carlo simulations of PT.

159   The results of this previous study dictated the physics models used in the PBS Monte Carlo code.

160   To model the electromagnetic interactions, the G4EmStandard (Agostinelli *et al.*, 2003) model was

161   used. This model governs the interactions of photons and all charged particles which have energy

162   greater than 1keV. The Bethe-Bloch equation is used for specifying the energy loss of hadrons of

163   energy greater than 2MeV. Inelastic hadronic interactions were modeled using a binary cascade

164   (G4BinaryCascadeFolger *et al.*, 2004) whilst the particle energy of is greater than 100MeV. Once the

165   energy of the particle falls below 100MeV, the precompound model (G4PreCompoundModel) is

166   invoked. Elastic interactions are governed by the UHElastic model (Ivanchenko, 2006).

167   The DS code previously developed by Paganetti *et al* (Paganetti *et al.*, 2004) has been shown to

168   predict absolute doses in water within an accuracy of 1.5% compared to ionization chamber

169   measurements (Paganetti, 2006). Since we have used the same physics models for the Monte Carlo

170   simulations in this study, one could expect comparable agreement using the PBS code for absolute

171   doses. The comparisons performed in this study only considered relative doses, which may lead to

172   better agreement than 1.5%.

173   In terms of secondary radiation, extensive validation of the nuclear models used in the Monte Carlo

174   has been previously undertaken through comparisons with Faraday cup measurements (Zacharatou

175   Jarlskog and Paganetti, 2008a). Direct comparison of the Monte Carlo doses with ionization chamber

176 measurements external to the primary field in proton therapy demonstrated the suitability of the

177 chosen physics models for simulation of out-of-field doses in PT (Clasie *et al.*, 2009).

178 *2.2. Calibration and validation of PBS Monte Carlo code*

179 Depth dose curves were measured using a plane-parallel chamber with an entrance window of

180 diameter 84mm (PTW Freiburg GmbH). The depth dose curves were measured in a water tank for

181 proton pencil beams at five different ranges, $8.92g/cm^2$, $12.64g/cm^2$, $15.92g/cm^2$, $21.1g/cm^2$ and

182 $25.15g/cm^2$. The energy spread of the beam at nozzle entrance was determined by minimizing the χ^2

183 of the Monte Carlo results against experimental data for different energies over the range of

184 therapeutic energies deliverable at MGH. Combining the specification of the energy distribution at

185 nozzle entrance with the Twiss parameters allows the specification of all properties of the proton

186 beam required for Monte Carlo simulations.

187 The lateral deviation of the proton beam from the central axis is directly related to the strength of the

188 magnetic field in the scanning magnets. The script used to convert lateral position to scanning magnet

189 field strength in the Monte Carlo code was verified to ensure that the lateral spot position observed in

190 simulations matched the position prescribed by the input file within 1mm at five different ranges,

191 $8.92g/cm^2$, $12.64g/cm^2$, $15.92g/cm^2$, $21.1g/cm^2$ and $25.15g/cm^2$.

192 The simulation of a complex two-dimensional test pattern was compared to measurements using a

193 Beam Imaging System (BIS) (Ion Beam Applications Dosimetry) at isocenter in air. The BIS uses a

194 30cm x 30cm scintillator and a CCD camera to capture the image. The energy deposition in the Monte

195 Carlo simulation was obtained at isocenter in air using a 30cm x 30cm x 0.2cm volume of water with

196 the front face placed at isocenter and the maximum step size restricted to 0.02mm. The lateral voxel

197 size used in both the Monte Carlo simulation and experimental measurement was 0.73mm x 0.73mm.

198 Monte Carlo simulations and experimental measurement where compared via gamma analysis (Low

199 *et al.*, 1998. The scanning pattern used in this comparison validates all aspects of the Monte Carlo

200 simulations (other than range), by combining position, spot size and dose delivery checks into a single

201 field.

202 Table 1 shows the different parameters considered in the PBS Monte Carlo code and the method of

203 calibration and/or validation.

204 **Table 1: Methods of calibration and validation of the different aspects of the PBS Monte Carlo**

205 **code used in this study. (MC = Monte Carlo, BIS = Beam Imaging System)**

Parameter	Configured and validated by
Proton range	Depth dose curves in water tank
Energy spread at nozzle entrance	Minimizing χ^2 of MC results against experimental measurement in water tank
Scanning magnet field strength	Measurement of lateral spot positions for different ranges using the BIS Complex 2D irradiation
Spot size	Calibration of Twiss parameters (α,β,γ) Complex 2D irradiation

206

207

208 *2.3. Monte Carlo simulations of clinical prostate field*

209 A prostate field was chosen because of the typically large range used in these treatments. The lateral

210 field size is defined in DS as the area contained within the projection of the patient-specific aperture

211 upon the phantom. The PBS field was generated to match the lateral dimensions of the DS field. The

212 PBS field had a range (R_{90}) of 22.8g/cm^2, a modulation (M_{90-90}) of 10.4g/cm^2 and a lateral field size of

213 45.2cm^2.

214 All simulations of the clinical prostate field were performed in two separate parts. In the first step, the

215 primary protons (and secondary particles) were transported through the treatment head (either DS or

216 PBS), resulting in the generation of a phase space file at nozzle exit which contained the energy,

217 position and direction of all particles which exited the treatment head. The properties phase space files

218 were then used to define the initial conditions of the second step which transported the particles from

219 nozzle exit into the phantom. The maximum step size was restricted to 0.2mm for all particles in the

220 phantom. Using the phase space allowed the field to be simulated upon the phantom multiple times

221 whilst requiring calculation of the particle transport through the treatment head only once, thereby

222 making the simulation process more time efficient. Each full simulation (treatment head and phantom)

223 took approximately 5 days to complete. This long simulation time was required to achieve acceptable

224 statistics in the scoring volumes distal to and at large lateral distances from the primary field.

225 In addition to conventional PBS, the aperture used in the DS simulations was placed at nozzle exit for

226 a series of PBS simulations. The primary fields were incident upon a Lucite phantom of size 90cm x

227 26cm x 37.76cm in all the simulations for all delivery techniques.

228 In addition to scoring volumes along the central axis, distances from the lateral field edge of 2.5cm,

229 5cm, 7.5cm, 10cm, 15cm, 20cm, 30cm, 40cm and 50cm were considered at depths of 4.72cm,

230 9.44cm, 14.16cm, 18.88cm, 23.6cm, 28.32cm and 33.04cm in Lucite. To increase statistics, larger

231 volumes were used out-of-field where the dose gradient is not as steep. The volume sizes varied based

232 on the lateral distance (x) from the field edge. The sizes used were 3.8 x 3.8 x 1.1 mm^3 (x $\leq$ 5cm), 7.6

233 x 7.6 x 1.1 mm^3 (5cm < x $\leq$ 20cm) and 15 x 15 x 1.1 mm^3 (x > 20cm) (see figure 3). A similar

234 methodology was adopted in the previous work of Clasie *et al* (2009).

235

236
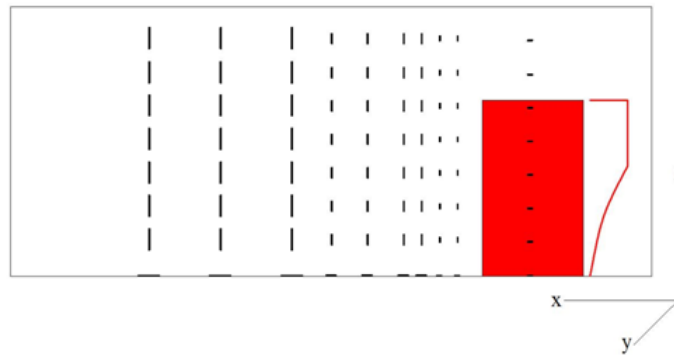
Figure 3: Diagram of the scoring volume positions simulated. The black rectangles show the position, orientation and relative size of the detector volumes. The size of the scoring volumes used varied based on the distance from the field edge (x) and were 1.1 x 3.8 x 3.8 mm^3 (x ≤ 5cm), 1.1 x 7.6 x 7.6 mm^3 (5cm < x ≤ 20cm) and 1.1 x 15 x 15 mm^3 (x > 20cm). The detectors at the phantom entrance and along the central axis were rotated by 90° so the majority of particles passed through the largest face of the scoring volumes. The colored area shows the section of the phantom irradiated by the primary field and a depth-dose curve demonstrates the modulation width of the SOBP.

The absorbed dose was obtained in each of the scoring volumes and separated based on particle type. This allowed application of particle specific weighting factors for low dose radiations. The absorbed dose due to protons (D_p), neutrons (D_n) and photons (D_γ) was tallied separately. Neutron energy spectra were also collected in 1MeV bins during the Monte Carlo simulations which allowed calculation of the average radiation weighting factor, w_R, based on the ICRP definition (ICRP 2003). The average neutron weighting factors were then used to convert the absorbed dose (D) to equivalent dose (H) using equation 6. Photons are given a factor of 1, whilst protons are assigned a factor of 2 to account for secondary particles which deposit dose locally such as δ-electrons and charged nuclear fragments (ICRP, 2003).

$$H = 2D_p + w_R D_n + D_\gamma \tag{6}$$

255

3. Results

3.1. Monte Carlo calibration and validation

3.1.1. Depth dose characteristics. Depth dose curves were measured using a plane-parallel chamber with an entrance window of diameter 84mm (PTW Freiburg GmbH) in a water tank for proton pencil beams of range, 8.92g/cm^2, 12.64g/cm^2, 15.92g/cm^2, 21.1g/cm^2 and 25.15g/cm^2 (see figure 4). The dose was scored in the Monte Carlo using cylindrical voxels of diameter 84mm and thickness 0.2mm to give high depth resolution and to match the lateral dimensions of the plane-parallel chamber. The results shown in figure 4 are the mean of 10 independent simulations which each cycled through their respective phase space files 5 times (total ~34 million particles transported into the phantom in each simulation). The uncertainty in the depth-dose curves was defined as the standard deviation of the 10 simulations and is less than 1% at all depths for all simulations. Emphasis was placed on taking measurements close to the Bragg peak and on the distal edge for range verification and calibration of the initial energy spread at nozzle entrance. The initial energy spread (ΔE) in terms of proton energy (E) was determined by comparigin experimental and simulated pristine Bragg curves and is given in equation 7.

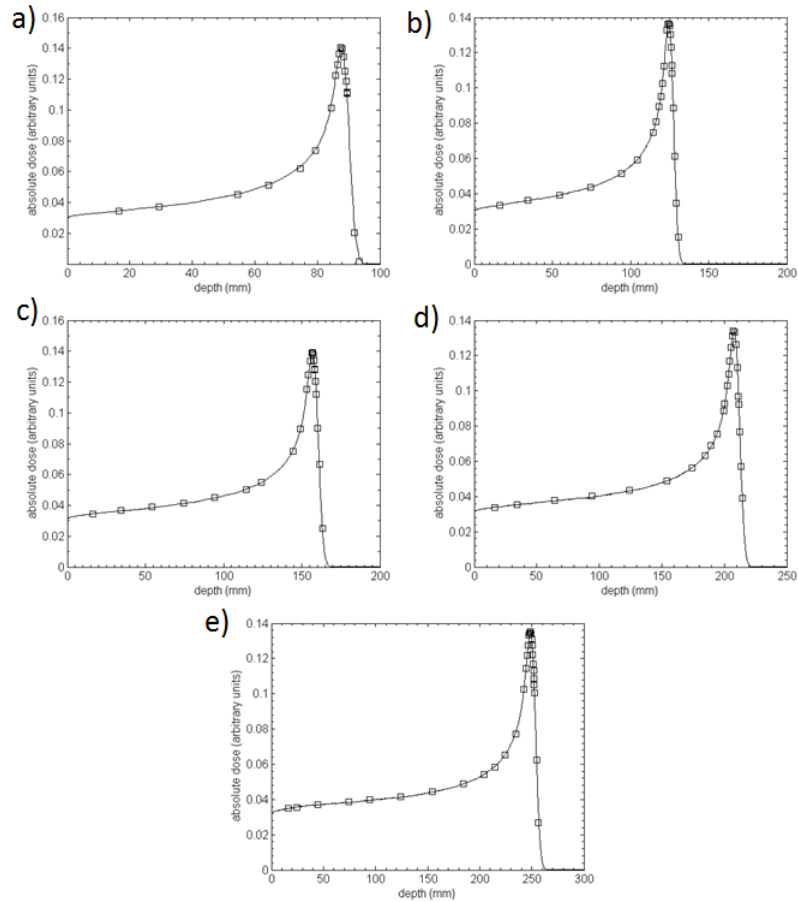$$\frac{\Delta E}{E}(\%) = 4.7 \times 10^{-5} E^2 - 0.021E + 2.60 \qquad (7)$$

279

Figure 4: Depth dose curves for (a) 8.92g/cm^2, (b) 12.64g/cm^2, (c) 15.92g/cm^2, (d) 21.1g/cm^2 and (e) 25.15g/cm^2. The solid line is the Monte Carlo data and the squares represent experimental data points. The uncertainty in the Monte Carlo is <1% at all points.

283

The results of the depth dose curves demonstrate good agreement between the measurement and simulation data.

3.1.2. Scanning magnet field strength. The magnetic field calibration was performed for beams of range 8.92g/cm^2, 12.64g/cm^2, 15.92g/cm^2, 21.1g/cm^2 and 25.15g/cm^2. These ranges correspond to nominal energies of 95.69MeV, 112.53MeV, 138.08MeV, 156.67MeV and 174.74MeV at nozzle entrance for the MGH PBS system, respectively. Five distinct spots were irradiated for each of the energies at different lateral positions (Figure 5). The results shown in Figure 5 are averages of 10
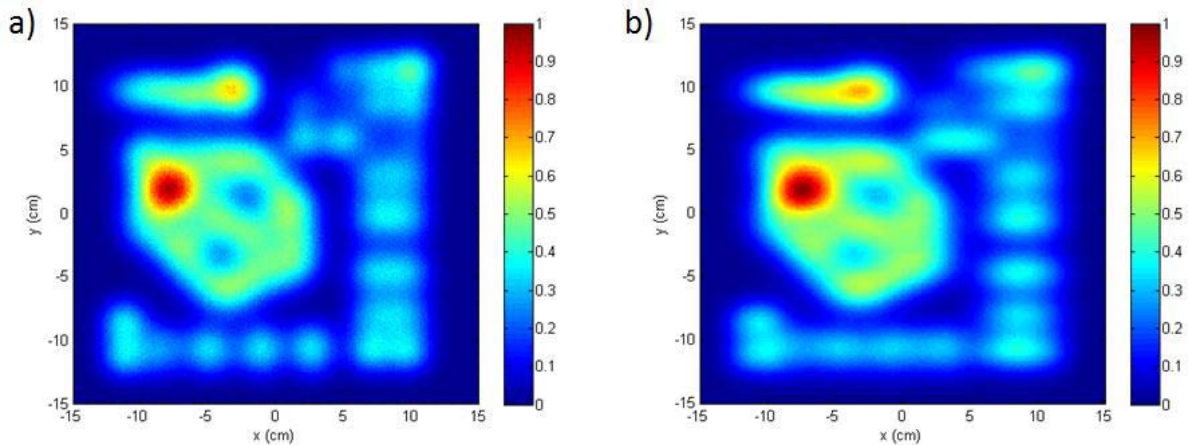
291   independent simulations, each containing ~34 million primary protons. The results shown in Figure 5

292   are a superposition of the 5 spots for the 5 different energies considered (i.e. total of 25 spots). The

293   lateral spot positions in the Monte Carlo matched those measured using the BIS within 1mm for each

294   considered energy, demonstrating that the conversion of lateral position to magnetic field strength

295   varies correctly with proton energy (and hence range).
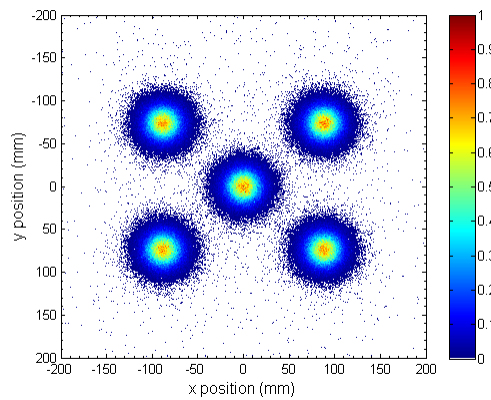
296

297   **Figure 5: Calibration of magnetic fields to control lateral position of the proton beam in the**

298   **Monte Carlo simulations. The units on the color scale are relative to the maximum observed**

299   **value. The data in the figure contains the 5 considered ranges (8.92g/cm^2, 12.64g/cm^2,**

300   **15.92g/cm^2, 21.1g/cm^2 and 25.15g/cm^2).**

301   *3.1.3. Complex two-dimensional irradiation.* Figure 6 shows the results of the Monte Carlo simulation

302   (a) and experimental delivery (b) of the test pattern.

303

Figure 6: Simulated (a) and measured (b) complex 2 dimensional irradiation containing areas of variable dose, continuous scanning and spot scanning.

The Monte Carlo simulation plot is an average of 10 independent simulations, each containing ~34 million primary protons. The uncertainty in the Monte Carlo data was less than 1% at all points considered. The dose was normalized to the maximum dose observed in both the simulated and experimental data. Relative doses were used rather than absolute as the BIS is not capable of measuring absolute dose. The simulated and measured results were compared via gamma analysis (Low *et al.*, 1998), with 100% of the points passing the 2mm/2% criteria.

*3.2. The impact of apertures in beam scanning on the example of a prostate treatment field*

3.2.1. Doses at depths proximal to the SOBP. At a depth of 4.72cm in Lucite, the absorbed dose at 2.5cm out-of-field was found to be approximately 3 times higher for PBS than DS. The reason lies in the relatively large spot size used in PBS at the MGH (~12mm at isocenter). At a depth of 9.44cm, DS shows close to 5 times higher doses than PBS. The latter is caused by secondary doses created in the aperture when using DS.

Including an aperture at nozzle exit reduces the penumbral width by preventing wide-angle scatter from reaching the phantom (or patient). At larger lateral distances from the field edge, the difference

321   in the doses between the considered delivery techniques increases. The absorbed dose from PBS with

322   an aperture is an order of magnitude lower than for the other techniques at 2.5cm from the field edge

323   at a depth of 4.72cm in water (see figure 7). For lateral distances less than 10cm from the field edge in

324   PBS, primary protons dominate the total equivalent dose. At greater lateral distances, the contribution

325   of scattered primary protons is not significant and the absorbed dose from PBS becomes less than DS.

326   As the absorbed dose at lateral distances from the field edge greater than 20cm is dominated by

327   internally produced secondary particles, the benefit of using an aperture is somewhat diminished in

328   such regions.
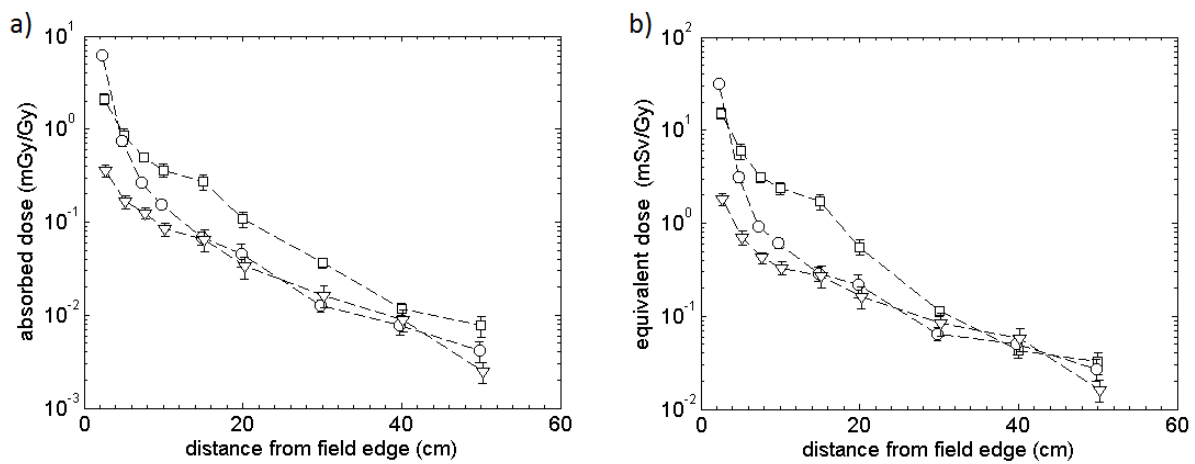
329

330   **Figure 7: Simulated absorbed dose (a) and equivalent dose (b) at different lateral distances from**

331   **the field edge at entrance depth of 4.72cm. The doses are relative to the absorbed dose delivered**

332   **in the SOBP. The data shown is for the double scattering (squares), pencil beam scanning**

333   **(circles) and pencil beam scanning with an aperture (triangles). The error bars represent two**

334   **standard deviations.**

335

336   *3.2.2. Doses at depths corresponding to the SOBP.* Figure 8 shows the absorbed dose and equivalent

337   dose at a depth of 18.88cm. The absorbed dose close to the field edge is again clearly higher in PBS

338   than the other considered delivery techniques. The absorbed dose from DS is higher than PBS at all

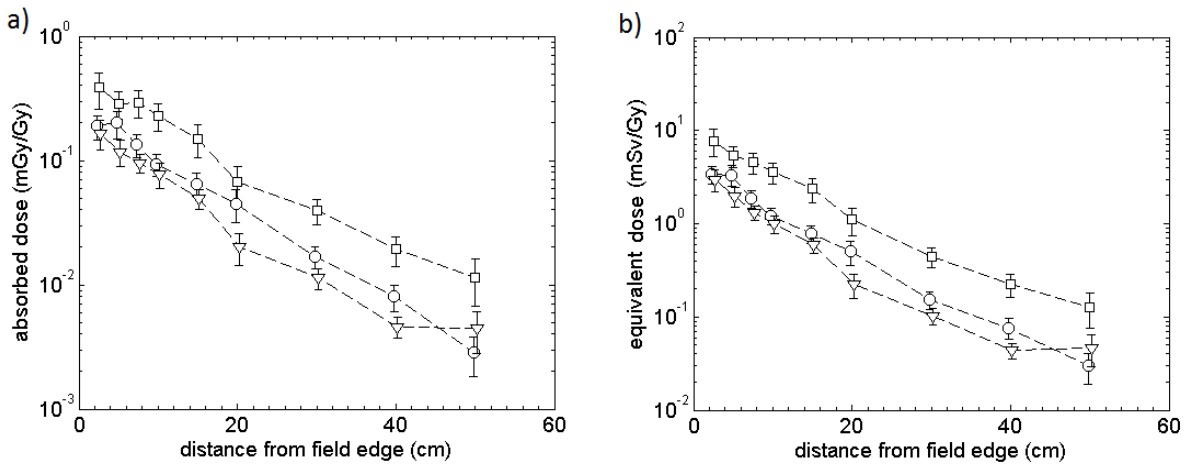339   lateral distances greater than 10cm from the field edge.

340
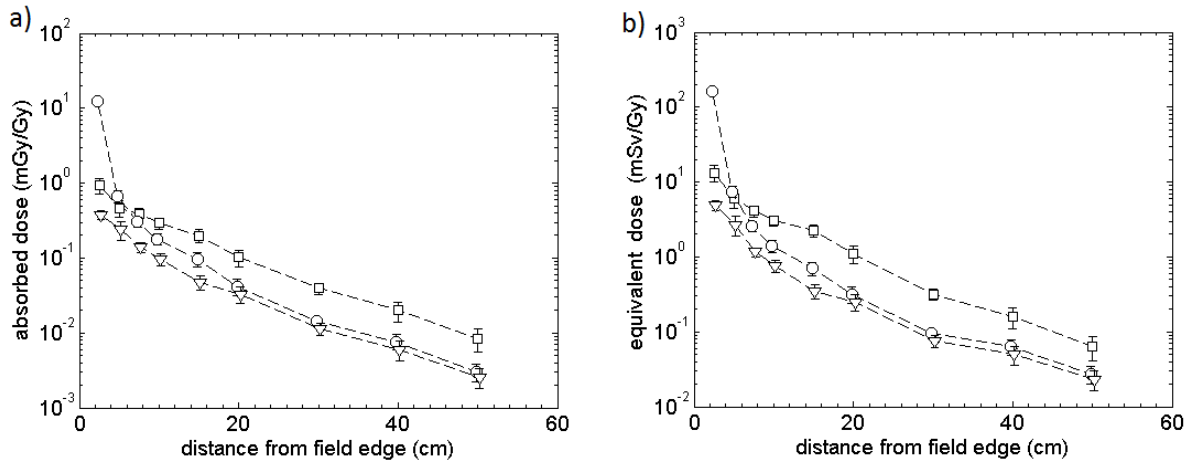
Figure 8: Simulated absorbed dose (a) and equivalent dose (b) for the double scattering (squares), pencil beam scanning (circles) and pencil beam scanning with an aperture (triangles) at a depth of 18.88cm. The doses are relative to the dose delivered in the SOBP. The error bars represent two standard deviations.

Using an aperture significantly reduces the absorbed dose from PBS for lateral distances up to 20cm from the field edge at depths within in the SOBP. At 2.5cm from the field edge, the absorbed dose is reduced by more than an order of magnitude when the aperture is used. For larger distances, the benefit of an aperture is not as pronounced due to the higher contribution of internally produced secondary and scattered particles to the total dose.

The equivalent dose curves agree within the uncertainty limits for the PBS and PBS with an aperture data for lateral distances greater than 20cm. The higher equivalent dose values observed for the DS data highlights the significant contribution of neutrons generated in the treatment head (in particular the aperture) for this delivery technique. The equivalent dose from DS is significantly higher than all other techniques for all lateral distances greater than 5cm from the field edge. Note that when using an aperture in PBS only a small portion of the field is restricted by the aperture while in DS typically the majority of the incident proton therapy field will be blocked by the aperture.

3.2.3. Doses at depths distal to the SOBP. The contribution of primary protons to the total absorbed dose and equivalent dose distal to the SOBP is zero due to their finite range. The absorbed dose and

359   equivalent dose values obtained distal to the SOBP (see figure 9) is entirely due to secondary

360   particles. The higher doses observed distal to the SOBP in DS are due to the higher number of

361   secondary particles generated in the treatment head compared to the other delivery techniques. As the

362   depth in the phantom increases, the relative contribution from internally generated secondary particles

363   to the total dose increases. The increased neutron fluence from DS contributes to a higher neutron

364   absorbed dose and equivalent dose compared to the other considered techniques. The increased

365   number of secondary particles, especially neutrons, incident upon the phantom in DS leads to an

366   increased production of secondary particles, the effect of which can still be observed distal to the

367   SOBP.

368

369   **Figure 9: Simulated absorbed dose (a) and equivalent dose (b) for the double scattering**

370   **(squares), pencil beam scanning (circles) and scanning with an aperture (triangles) at a depth of**

371   **28.32cm. The dose values are relative to the dose delivered in the SOBP. The error bars**

372   **represent two standard deviations.**

373

374   **4. Discussion and Conclusion**

375   Placing a patient-specific aperture at nozzle exit reduces the out-of-field doses from PBS. Proton

376   interactions occurring in the brass of the aperture lead to a higher neutron fluence compared to PBS

377   with no aperture. The neutron component of the total dose out-of-field increases when using an

378 aperture in PBS, however the total doses are still reduced. The reduction in the dose from primary

379 protons, due to the large angle scatter not reaching the phantom leads to a reduction in the total

380 absorbed dose and equivalent dose when an aperture is placed at nozzle exit. The number of proton

381 interactions in the aperture is much lower in PBS than in DS. In DS, a large proportion of the primary

382 beam interacts with the aperture, leading to a high neutron and secondary particle fluence. In PBS, a

383 comparatively small amount of interactions occur in the aperture, as the majority of the primary

384 protons pass through the aperture without undergoing an interaction. The aperture only interacts with

385 particles which have been scattered through large angles.

386 The benefit of incorporating an aperture in PBS is diminished distal to the SOBP. Some benefit can

387 still be observed distal to the SOBP, demonstrated by the reduced absorbed doses and equivalent

388 doses in this region compared to PBS with no aperture. The reduction in the penumbral width reduces

389 the proton fluence and dose lateral to the primary field in PBS. This reduction in proton fluence leads

390 to a decrease in secondary particle production, the effect of which can be seen in the lower out-of-

391 field doses throughout the phantom compared to PBS with no aperture.

392 One of the reasons for moving to PBS in preference to DS is the removal of the dependency upon

393 patient-specific hardware, which adds to the cost of operating a clinical proton facility. However, one

394 of the issues with scanning is the wider penumbra when the pencil beam width is large and/or the

395 proton energy is small, which is demonstrated in the simulation results presented here. The use of a

396 patient-specific aperture may be required to decrease the penumbral width for certain clinical cases,

397 but the other advantages of PBS compared to DS will still be largely maintained. The results of the

398 simulations in this work show that using an aperture can potentially reduce the absorbed dose and

399 equivalent dose lateral to the primary field in PBS by an order of magnitude.

400

References

Agostinelli S, *et al.* 2003 Geant4—a simulation toolkit *Nuclear Inst. and Methods in Physics Research, A* **506** 250-303

Bednarz B and Paganetti H 2010 Reducing uncertainties in the dose distributions of small proton fields using Monte Carlo calculations. In: *PTCOG49,* (Japan

Brown K L, Carey D C, Iselin C and Rothacker F 1980 Transport, a Computer Program for Designing Charged Particle Beam Transport Systems *Yellow Reports CERN 73-16 (1973) & CERN 80-04 (1980)*

Clasie B, Wroe A, Kooy H, Depauw N, Flanz J, Paganetti H and Rosenfeld A 2009 Assessment of out-of-field absorbed dose and equivalent dose in proton fields *Med Phys* **37** 311-21

Dowdell S, Clasie B, Wroe A, Guatelli S, Metcalfe P, Schulte R and Rosenfeld A 2009 Tissue equivalency of phantom materials for neutron dosimetry in proton therapy *Med Phys* **36** 5412-9

Folger G, Ivanchenko V N and Wellisch J P 2004 The Binary Cascade *The European Physical Journal A-Hadrons and Nuclei* **21** 407-17

Hall E J 2006 Intensity-modulated radiation therapy, protons, and the risk of second cancers *Int J Radiat Oncol Biol Phys* **65** 1-7

ICRP 2003 Relative Biological Effectiveness (RBE), Quality Factor (Q), Radiation Weighting Factor (wR).

Ivanchenko V N 2006 Combined cross-sections and elastic scattering. In: *11th Geant4 Collaboration Workshop and Users Conf.,* (Lisbon, Portugal

Kooy H M, *et al.* 2010 A case study in proton pencil-beam scanning delivery *Int J Radiat Oncol Biol Phys* **76** 624-30

Lomax A J, Pedroni E, Rutz H and Goitein G 2004 The clinical potential of intensity modulated proton therapy *Z Med Phys* **14** 147-52

Low D A, Harms W B, Mutic S and Purdy J A 1998 A technique for the quantitative evaluation of dose distributions *Med Phys* **25** 656-61

Paganetti H 2002 Nuclear interactions in proton therapy: dose and relative biological effect distributions originating from primary and secondary particles *Phys Med Biol* **47** 747-64

Paganetti H 2006 Monte Carlo calculations for absolute dosimetry to determine machine outputs for proton therapy fields *Phys Med Biol* **51** 2801-12

Paganetti H, Jiang H, Lee S Y and Kooy H M 2004 Accurate Monte Carlo simulations for nozzle design, commissioning and quality assurance for a proton radiation therapy facility *Med Phys* **31** 2107-18

Paganetti H, Jiang H, Parodi K, Slopsema R and Engelsman M 2008 Clinical implementation of full Monte Carlo dose calculation in proton beam therapy *Phys Med Biol* **53** 4825-53

Perez-Andujar A, Newhauser W D and Deluca P M 2009 Neutron production from beam-modifying devices in a modern double scattering proton therapy beam delivery system *Phys Med Biol* **54** 993-1008

446   Peterson S W, Polf J, Bues M, Ciangaru G, Archambault L, Beddar S and Smith A 2009 Experimental
447   validation of a Monte Carlo proton therapy nozzle model incorporating magnetically steered
448   protons *Phys Med Biol* **54** 3217-29
449   Rohrer U 2007 PSI Graphic Transport Framework based on a CERN-SLAC-FERMILAB version by
450   K. L. Brown et al
451   Schneider U, Agosteo S, Pedroni E and Besserer J 2002 Secondary neutron dose during proton
452   therapy using spot scanning *Int J Radiat Oncol Biol Phys* **53** 244-51
453   Zacharatou Jarlskog C, Lee C, Bolch W E, Xu X G and Paganetti H 2008 Assessment of organ-
454   specific neutron equivalent doses in proton therapy using computational whole-body age-
455   dependent voxel phantoms *Phys Med Biol* **53** 693-717
456   Zacharatou Jarlskog C and Paganetti H 2008a Physics Settings for Using the Geant4 Toolkit in Proton
457   Therapy *IEEE Transactions on Nuclear Science* **55** 1018-25
458   Zacharatou Jarlskog C and Paganetti H 2008b Sensitivity of different dose scoring methods on organ-
459   specific neutron dose calculations in proton therapy *Phys Med Biol* **53** 4523-32
460
461

462